Stable Squares and Other Oscillatory Turing Patterns in a Reaction-Diffusion Model

Lingfa Yang, Anatol M. Zhabotinsky, and Irving R. Epstein*

Department of Chemistry and Volen Center for Complex Systems, MS 015, Brandeis University, Waltham, Massachusetts 02454-9110, USA

(Received 21 January 2004; published 13 May 2004)

We study the Brusselator reaction-diffusion model under conditions where the Hopf mode is supercritical and the Turing band is subcritical. Oscillating Turing patterns arise in the system when bulk oscillations lose their stability to spatial perturbations. Spatially uniform external periodic forcing can generate oscillating Turing patterns when both the Turing and Hopf modes are subcritical in the autonomous system. Most of the symmetric patterns show period doubling in both space and time. Patterns observed include squares, rhombi, stripes, and hexagons.

DOI: 10.1103/PhysRevLett.92.198303 PACS numbers: 82.40.Ck, 47.54.+r, 89.75.Kd

Although hexagonal structures are more commonly encountered, square patterns have been found in a variety of nonequilibrium systems. They arise as Faraday waves due to parametric forcing of layers of liquid [1] and sand [2]. They are formed by convective cells in Rayleigh-Bénard [3–5] and Marangoni-Bénard [6] convection. They have also been observed in ferrofluids [7,8] and nonlinear optical systems with feedback [9,10]. Square patterns have been found in a model of CO oxidation on Pt(100) with "up-hill" diffusion [11], and in the Swift-Hohenberg equation [12], where in both cases fourth-order spatial coupling is present. To the best of our knowledge, however, stable square patterns have not previously been obtained either in experiments on, or as stable solutions of, reaction-diffusion systems. Here we report observations of various oscillating Turing patterns, including stable squares, in the Brusselator model. These patterns arise from interaction between a subcritical Turing mode and bulk oscillations in the autonomous system. They can also be obtained by spatially uniform external periodic forcing when both the Turing and Hopf modes are subcritical.

We employ mainly the original Brusselator reaction-diffusion model [13]. When the only stable state of the autonomous system ($\alpha = 0$) is the uniform steady state, we add external uniform periodic forcing of frequency f ($\alpha \neq 0$) in order to study pattern formation:

$$\frac{\partial u}{\partial t} = a - (b+1)u + u^2 v + \alpha \cos(2\pi f t) + D_u \nabla^2 u, \quad (1)$$

$$\frac{\partial v}{\partial t} = bu - u^2 v + D_v \nabla^2 v, \quad (2)$$

Figure 1(a) shows the stability diagram of the spatially uniform steady state (SS) of the autonomous system in the (b, D_u) plane. The Hopf bifurcation line (H) is horizontal at $b = 10.0$. It crosses the Turing bifurcation line (T) at $D_u = 5.19$. Both bifurcations are supercritical. We study the behavior of the system in the oscillatory and oscillatory Turing ($\lambda_T > 0$, $\mathrm{Re}\lambda_H > 0$) domains at constant supercriticality, $b = 10.2$. Figure 1(b) shows the dispersion curves at the designated points in Fig. 1(a).

All our simulations employ periodic boundary conditions with a system size of 128×128 space units. Grey levels show concentration of u. Figure 2(a) shows snapshots of the stable patterns at the same set of points. If $D_u > 6.3$, the system generates uniform bulk oscillations (BO). When D_u is about 6.0, oscillating square patterns arise [Fig. 2(a)-2]; oscillating hexagons [Fig. 2(a)-3]

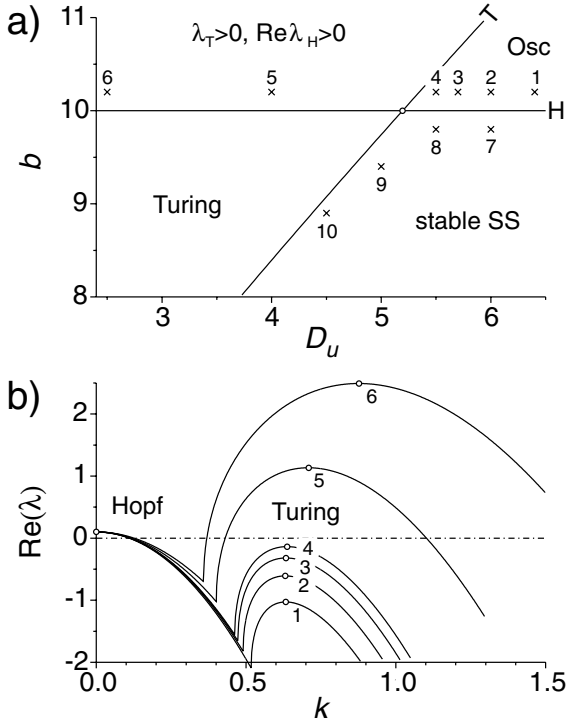

FIG. 1. Stability analysis of the Brusselator model. (a) Bifurcation diagram. Hopf bifurcation: $b_c^H = 1 + a^2$; Turing bifurcation: $b_c^T = [1 + a\sqrt{D_u/D_v}]^2$, with fixed $a = 3$, $D_v = 10$. (b) Dispersion relations showing unstable Hopf mode and transition of Turing mode from stable to unstable, e.g., as D_u is decreased.

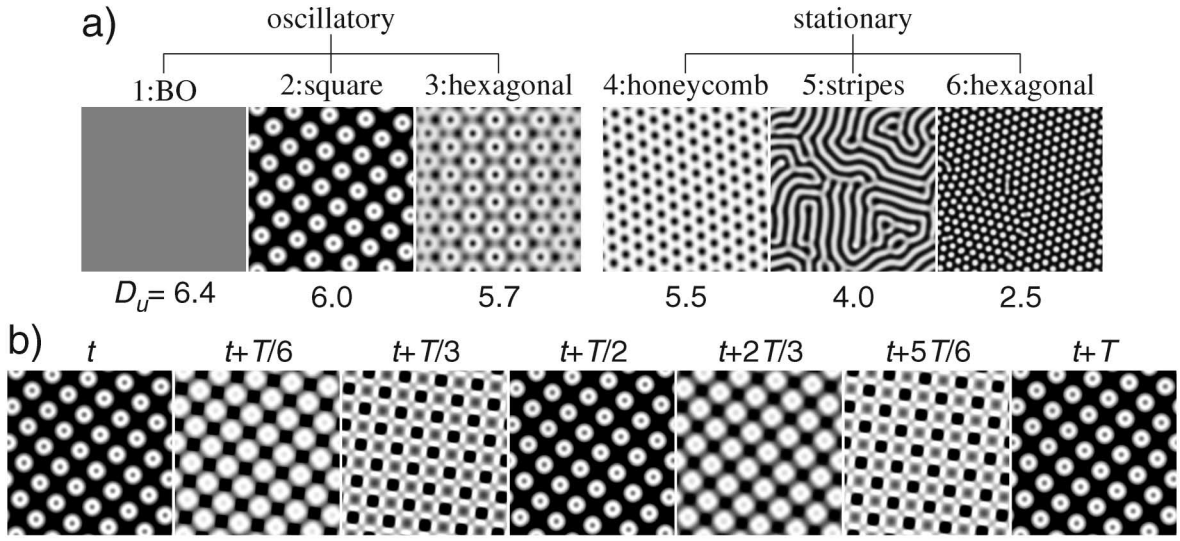

FIG. 2. (a) Pattern scenario with growth of the Turing instability as shown as marked points 1–6 in Fig. 1. Oscillatory patterns include BO (1), square (2), or hexagonal (3) lattices. Stationary patterns include honeycomb (4), stripes (5), and hexagonal spots (6). (b) One full period of the oscillatory square.

appear at about $D_u = 5.7$. Both of these patterns are superlattices. As we decrease D_u, regular stationary Turing patterns emerge: honeycomb hexagonal patterns [Fig. 2(a)-4], giving way to labyrinthine patterns [Fig. 2(a)-5] and then to inverted hexagons [Fig. 2(a)-6].

The oscillating superlattice patterns are double periodic both in time and in space. They are related to the oscillatory patterns found earlier in the spatially one-dimensional Brusselator model near the codimension-two Hopf-Turing point in the region where both modes are supercritical [14]. Here, the patterns occur in the oscillatory domain far from the Turing line. Some criteria for the existence of stable square Turing patterns have been obtained previously in the framework of amplitude equations [15,16], but we have not been able to find any demonstration of such patterns in reaction-diffusion models. Hence, we studied this phenomenon in more detail. Figure 2(b) shows an entire period of oscillation of the square lattice. The time period is twice the period of the BO. One can see that the instantaneous patterns shifted by half a time period are shifted by half a space period along both principal axes. Fourier spectra of the pattern reveal three major spatial modes with wave numbers $k_T/2$, $k_T/\sqrt{2}$, and k_T. The fundamental wave number k_T is shifted slightly to the left of the maximum of the Turing band in Fig. 1(b)-2. In some parts of the oscillatory cycle only one of the modes, $k_T/2$ or $k_T/\sqrt{2}$, has a significant amplitude, while the amplitude of mode k_T is always large.

This square pattern is quite robust, occurring in a significant domain of the parametric space ($2.4 < a < 3.5$, and $b_c^H < b < b_c^T$). It survives addition of a small term of mutual annihilation of activator and inhibitor, $-uv$, to the Brusselator. We have also found this pattern in the Sel'kov model [17] in an analogous region of the bifurcation diagram. The oscillatory hexagonal lattice with phase modulation in Fig. 2(a)-3 is observed in a narrow range of parameters and, similar to the square lattice, also shows double periodicity. Earlier, we found a period tripling version of this pattern [18].

Evolution from the initial condition, the randomly perturbed uniform SS, to a specific stable pattern in Fig. 2(a) depends on the position of the system in the parameter space. When the system is in the oscillatory domain between the Hopf and Turing lines, spatially uniform bulk oscillations [Fig. 2(a)-1] develop initially. Then, spatial modulation of the BO appears with approximately twice the wavelength of the maximum of the Turing band, leading to the final stable oscillatory pattern [Figs. 2(a)-2 and 2(a)-3]. When the parameters lie in the domain above both the Hopf and Turing lines [Figs. 2(a)-5 and 2(a)-6], the stationary Turing patterns start to develop immediately from the random initial conditions. Formation of the pattern in Fig. 2(a)-4, near the codimension-two point, is more complex. On the one hand, spatial perturbations around the SS tend to decay, because all spatial modes at the SS are damped. Thus, BO develops first. On the other hand, once the BO emerges, it activates the Turing mode, and the Turing pattern grows, ultimately supplanting the BO.

Oscillating Turing patterns can also be produced in the system where both the Turing and Hopf modes at SS are subcritical, if the system is subjected to external periodic forcing, $\alpha > 0$ in Eq. (1). Figure 3 illustrates the pattern formation at point 7 in Fig. 1(a). Figure 3(a) shows a frequency-amplitude diagram, where a tongue-shaped domain of oscillating patterns is surrounded by an area of BO. Figure 3(b) contains a typical sequence of patterns arising when the frequency is decreased along the arrow shown in Fig. 3(a). Figure 3(b)-1 shows a square pattern,

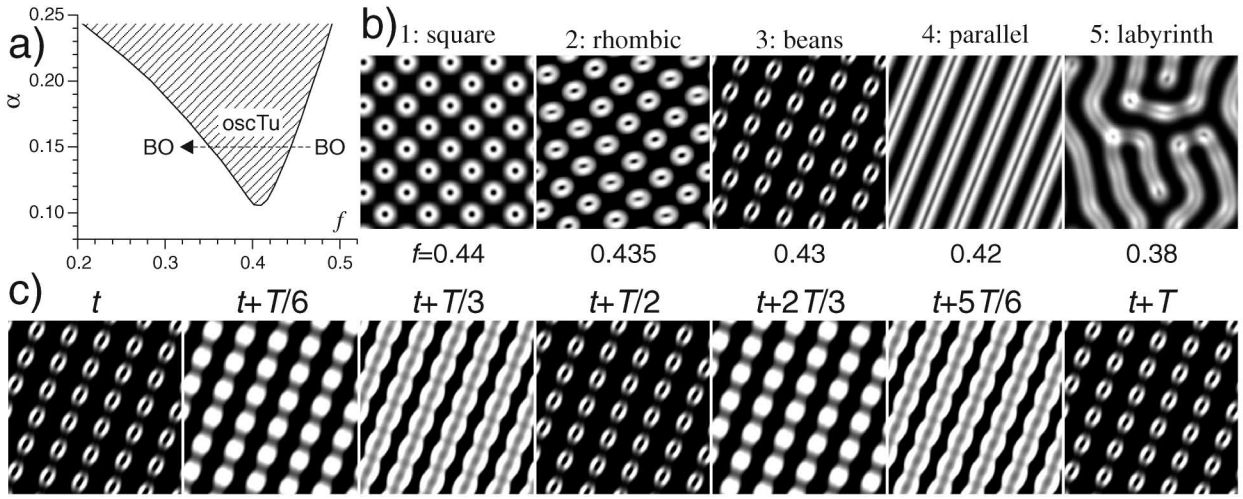

FIG. 3. Oscillatory Turing patterns under periodic forcing. (a) Pattern locking diagram in frequency f, and forcing strength α. (b) Scenario as f is decreased along arrow in (a), square (1), and rhombic (2) lattices; modulated (3), parallel (4), and labyrinthine (5) stripes. (c) One full period of the modulated stripe pattern.

Fig. 3(b)-2 shows a rhombic pattern, and Fig. 3(b)-3 shows a pattern of strongly modulated parallel stripes. An entire oscillation cycle of this last pattern is shown in Fig. 3(c). Figure 3(b)-4 shows a parallel stripe pattern which is stable around $f = 0.42$. Labyrinthine patterns occupy the remainder of the domain. This sequence of patterns is found at $\alpha = 0.12$, 0.15, 0.17, and 0.20.

With similar forcing, we find oscillating hexagonal superlattices, parallel stripes, and labyrinthine patterns at point 8 in Fig. 1(a). Labyrinthine patterns appear at points 9 and 10. Hexagons were also found at point 10.

The linear stability analysis used to generate Fig. 1 applies only to the stability of the uniform steady state to spatiotemporal perturbation. To understand better the stability properties of the BO, we need to examine the Floquet multipliers associated with the limit cycle solution. The Floquet multipliers $\mu_{1,2}$ of the limit cycle calculated as a function of the wave number k are shown in Fig. 4. At $k = 0$, the nontrivial multiplier (point A) is less than 1 in absolute value, indicating that the limit cycle is orbitally asymptotically stable. The limit cycle loses stability at $k_0 = 0.32$, where the dominant multiplier crosses -1. This crossing corresponds to the period doubling bifurcation, because any T-periodic function $P(t)$ around the limit cycle now obeys $P(t + T) = -P(T)$, $P(t + 2T) = P(T)$.

In Fig. 4, the system is very close to the period doubling bifurcation point and has essentially a single unstable spatial mode at k_0. Its second harmonic, $2k_0$, is near the maximum of the curve $\mu(k)$. Comparison with the results of direct simulations, shown in Fig. 2, reveals that $2k_0 = k_T$. Thus, this harmonic of the primary unstable mode determines the principal space scale of the oscillatory square pattern, and combines with the modes at k_0 and $\sqrt{2}k_0$ to generate the superlattice. The maximum of the curve $\mu(k)$ is close to the maximum of the Turing band in Fig. 1(b). The temporal period doubling that takes place at k_0 produces a standing wave of that wave number. One can thus view the development of the spatial structure either as a result of the 1:2 resonance between this standing wave and the Turing mode or as a 1:1 resonance between two stationary entities: the envelope of the standing wave and the Turing mode.

As we move along the line of points $1 \rightarrow 2 \rightarrow 3 \rightarrow 4$ in Fig. 1, the slave mode at $2k_0$ grows and $\mu(k)$ in Fig. 4 reaches 1 before the Turing instability of the steady state occurs in Fig. 1. This difference in behavior between the eigenvalues of the Jacobian matrix and the Floquet multipliers explains why we obtained a *stationary* Turing pattern in Fig. 2(a)-4 even though the Turing instability at that point is still below criticality.

We have shown in a reaction-diffusion model how interaction with a subcritical Turing mode can destabilize uniform bulk oscillation and lead to either oscillatory

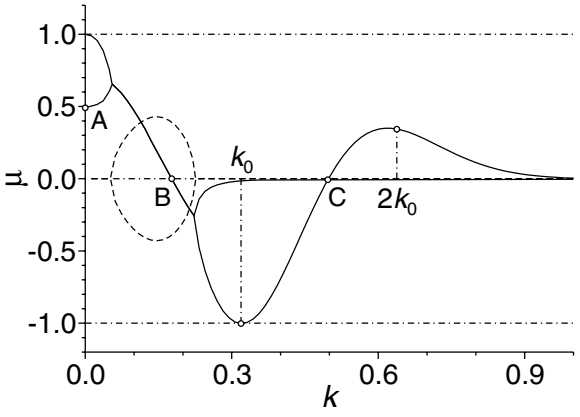

FIG. 4. Floquet multipliers $\mu_{1,2}$ (solid for real; dashed for imaginary part) of the limit cycle solution as a function of wave number k. Parameters as in Fig. 1(a)-2.

or stationary Turing patterns. In particular, stable square patterns, which have not previously been seen in reaction-diffusion systems, are obtained, and our results suggest how one might generate such patterns experimentally. For example, in the chlorite-iodide-malonic acid system [19] in a gel reactor, one might start at parameters just above the bifurcation from uniform steady state to bulk oscillations and then gradually vary the reservoir concentrations to approach the Turing bifurcation [analogous to moving from point 1 toward point 4 in Fig. 1(a)]. We have also seen that the standard linear stability analysis of the uniform steady state is insufficient to describe these phenomena and that one must carry out a Floquet analysis of the stability of the limit cycle under spatiotemporal perturbations. While the nature of the bifurcations involved is quite different, particularly with regard to wavelength selection, the behavior described here is analogous in a sense to the "self-parametric instability" of uniform bulk oscillations described by Argentina *et al.* [20] when the limit cycle approaches an Andronov homoclinic bifurcation.

This work was supported by the National Science Foundation under Grant No. CHE-0306262. We thank Bard Ermentrout for enlightenment about Floquet multipliers in the presence of spatial perturbations.

*Electronic address: epstein@brandeis.edu

[1] A. Kudrolli and J. P. Gollub, Physica (Amsterdam) **97D**, 133 (1996).
[2] P. B. Umbanhowar, F. Melo, and H. L. Swinney, Physica (Amsterdam) **249A**, 1 (1998).
[3] P. Le Gal, A. Pocheau, and V. Croquette, Phys. Rev. Lett. **54**, 2501 (1985).
[4] E. Moses and V. Steinberg, Phys. Rev. Lett. **57**, 2018 (1986).
[5] P. Le Gal and V. Croquette, Phys. Fluids **31**, 3440 (1998).
[6] M. F. Schatz, S. J. VanHook, W. D. McCormick, J. B. Swift, and H. L. Swinney, Phys. Fluids **11**, 2577 (1999).
[7] A. G. Boudouvis, J. L. Puchalla, L. E. Scriven, and R. E. Rosensweig, J. Magn. Magn. Mater. **65**, 307 (1987).
[8] H. J. Pi, S. Park, J. Lee, and K. J. Lee, Phys. Rev. Lett. **84**, 5316 (2000).
[9] G. K. Harkness *et al.*, J. Opt. B **1**, 177 (1999).
[10] T. Ackemann and T. Lange, Appl. Phys. B **72**, 21 (2001).
[11] J. Verdasca, P. Borckmans, and G. Dewel, Phys. Rev. E **64**, 055202 (2001).
[12] J. Buceta, K. Lindenberg, and J. M. R. Parrondo, Phys. Rev. Lett. **88**, 024103 (2002).
[13] I. Prigogine and R. Lefever, J. Chem. Phys. **48**, 1695 (1968).
[14] A. DeWit, D. Lima, G. Dewel, and P. Borckmans, Phys. Rev. E **54**, 261 (1996).
[15] B. A. Malomed and M. I. Tribelsky, Sov. Phys. JETP **65**, 305 (1987).
[16] P. Borckmans, G. Dewel, A. DeWit, and D. Walgraef, in *Chemical Waves and Patterns*, edited by R. Kapral and K. Showalter (Kluwer, Dordrecht, 1995), p. 323.
[17] E. E. Sel'kov, Eur. J. Biochem. **4**, 79 (1968).
[18] L. F. Yang, M. Dolnik, A. M. Zhabotinsky, and I. R. Epstein, Phys. Rev. Lett. **88**, 208303 (2002); L. F. Yang, and I. R. Epstein, Phys. Rev. Lett. **90**, 178303 (2003).
[19] I. Lengyel and I. R. Epstein, Science **251**, 650 (1991); **259**, 493 (1993).
[20] M. Argentina, P. Coullet, and E. Risler, Phys. Rev. Lett. **86**, 807 (2001).